American Mineralogist, Volume 98, pages 582–587, 2013

Quartz nanocrystals in the 2.48 Ga Dales Gorge banded iron formation of Hamersley, Western Australia: Evidence for a change from submarine to subaerial volcanism at the end of the Archean

Yi-Liang Li,[1,*] David R. Cole,[2] Kurt Konhauser,[3] and Lung Sang Chan[1]

[1]Department of Earth Sciences, The University of Hong Kong, Hong Kong, Special Administrative Region of China
[2]School of Earth Sciences, Ohio State University, Columbus, Ohio 43210, U.S.A.
[3]Department of Earth and Atmospheric Sciences, The University of Alberta, Edmonton, Alberta T6G 2E3, Canada

Abstract

Banded iron formations (BIF) have recently been used as proxies for tracking the chemical changes associated with the transition from an anoxic to oxic atmosphere around 2.45 billion years ago, known as the Great Oxidation Event (GOE). The timing of the GOE has been ascribed to both the collapse of a methane greenhouse and a decreased overall demand for oxygen due to the production of more oxidizing gases associated with greater subaerial volcanism. The latter is a byproduct of a period of high mantle plume activity and the formation of new continental crust between 2.51 to 2.45 Ga. Here we report unique mineral evidence for momentary subaerial volcanism recorded in hematite-rich layers of the 2.48 Ga BIF from Dales Gorge, Hamersley of Western Australia. The BIF contains euhedral quartz nanocrystals (QNC), which only occur on the surfaces or in cavities of hematite breccias exhibiting soft-sediment features and an exogenous source. These QNCs with an average size of 170–100 nm are distinct to the amorphous chert in the BIF mineral assemblage and have the smallest crystal sizes of well-crystallized quartz ever reported. We suggest that QNCs represent pyroclastic materials that were transported as dust particles to the BIF depositional setting. Although the analysis of one specific BIF unit does not provide proof of changing modes of volcanism during the Archean-Paleoproterozic transition, this high-resolution petrological study does confirm that subaerial volcanism existed at that time.

Keywords: Banded iron formation, chert, quartz nanocrystal, subaerial volcanism, rise of atmospheric oxygen

Introduction

Superior-type banded iron formations are layered chemical precipitates that developed in near-shore continental shelf environments and are typically interbedded with carbonates and black shales. Banding can be observed on a wide range of scales, from coarse macrobands (meters in thickness) to mesobands (centimeter-thick units) to millimeter and submillimeter layers (Trendall and Blockley 1970). Among the macrobands, the layers are commonly subdivided on the basis of mineralogy, with "BIF" macrobands dominated by iron oxides (e.g., hematite, magnetite) and chert or carbonate (siderite, dolomite-ankerite) and "S" macrobands comprising chert-carbonate-silicate BIF interspersed with shaley horizons (Morris 1993). The BIF macrobands are widely accepted as being chemical precipitates, formed initially of a mixture of ferric hydroxide [$Fe(OH)_3$], greenalite [$Fe_3Si_2O_5(OH)_4$], siderite ($FeCO_3$), and amorphous silica ($SiO_2 \cdot nH_2O$) (e.g., Klein 2005); these primary minerals have since been modified by both diagenetic and metamorphic processes. By contrast, the S macrobands, such as in the 2.48 Ga Penge Iron Formation South Africa, are believed to have been deposited when clastic materials were transported during a sea level drop into what was previously a sediment-starved, chemical precipitation environment (Bau and Dulski 1996).

Interestingly, in the 2.48 Gyr Dales Gorge Member of the Brockman Iron Formation, Western Australia, the S macrobands have instead been suggested to have been derived from subaerial pyroclastic input on normal BIF chemical processes. The S macrobands contain about 40–45% shale, which is made up of stilpnomelane and chlorite, with varying amounts of feldspar, mica, quartz, carbonates, carbonaceous material, and sulfides. A volcanogenic origin to the shales was proposed based on their lateral stratigraphic continuity and chemical composition (Trendall and Blockley 1970; Ewers and Morris 1981), although the only direct evidence of pyroclastic material is a few putative volcanic shards (La Berge 1966). During S macroband accumulation, total annual silica precipitation increased, as did the ratio of silica to iron. This increase has been attributed to surface cooling associated with "volcanic winters," and hence of supersaturation of warm incoming silica saturated water (Morris 1993).

The potential presence of pyroclastic material in the Dales Gorge BIF also has significant implications for global tectonic evolution during the Late Archean to early Palaeoproterozoic and the rise of atmospheric oxygen. Several studies have suggested that extensive igneous activity and the rapid growth of continents led to the change of atmospheric redox conditions

* E-mail: yiliang@hku.hk

0003-004X/13/0004–582$05.00/DOI: http://dx.doi.org/10.2138/am.2013.4205

and consequently the irreversible oxidation of the atmosphere (e.g., Kasting et al. 1993; Kump et al. 2001; Barley et al. 2005; Holland 2006). Specifically, Kump and Barley (2007) proposed that the transition from extensively submarine to subaerial volcanism occurred within a narrow time window, near 2.5 Ga, which might have changed the atmospheric composition and favored the stability of free O_2. Campbell and Allen (2008) supported the important role of supercontinent formation but stressed that the accelerated erosion of mountains provided more nutrients for photosynthesis and led to a high burial rate of organic matter, which in turn, allowed for atmospheric O_2 levels to increase.

In light of the importance of the Archean-Paleoproterozoic transition in terms of the evolution of Earth's surface system, we investigated core samples from the Dales Gorge Member (Li et al. 2011). The BIF has been extensively described in terms of its age, petrology, chemical composition, and likely depositional environment (e.g., Trendall and Blockley 1970; Ewers and Morris 1981; Morris 1993; Pickard 2002; Trendall et al. 2004; Pecoits et al. 2009), but as far as we are aware, no high-resolution studies have been conducted on its mineralogy and texture. In this study, we show that a component of quartz in the BIF was likely pyroclastic in nature, supporting the contention that subaerial volcanism existed at that time.

Methods

For the observation of hematite bands in BIF, samples were ground to micrometer sizes and immersed in water to make a hematite suspension. The silica fraction and magnetite crystals were separated either by their rapid setting or response to a permanent magnet. Fine-grained hematite particles collected from the suspension were observed by Hitachi S-4800 FEG scanning electron microscope (SEM) under secondary electron (SE) mode at low voltage (3–5 kV) for surface structures. As the BIFs are mostly made of micrometer- to nanometer-scaled minerals with their textural structures prone to be altered quickly by interaction with liquid, such as water, we also produce fresh surface without any treatment for direct observation. To do so, the centimeter-scaled specimens were polished to a surface roughness of 200 nm and then bladed the edge with a screwdriver to peel off thin flakes that produced conchoidal, concave surfaces for immediate and direct observation under scanning electron microscopes to avoid contamination. These samples were observed with backscatter electron (BSE) mode for interrogation of electron density heterogeneities, which differentiates mineralogical texture features. The chemical compositions were determined by energy-dispersive X-ray spectroscopy (EDS) at 20 kV. To extract the ultrafine siliceous minerals incorporated in hematite, the latter was treated by 6 M HCl overnight to dissolve iron oxides completely; the relics were then washed by pure water and dried at room temperature. The Tecnai G2 20 S-TWIN transmission electron microscope (STEM) equipped with EDS was used to characterize the structures of ultrafine minerals by selected-area electron diffraction (SAED) along with the observation of morphology and the measurement of chemical composition.

Results

In the BIF sample, the thicknesses of silica bands range from meter-scaled macrobands to micrometer-scaled microbands that alternate with hematite-rich microbands (Trendall 2002). Figure 1a shows a BSE image of chert (dark in color) and alternating hematite microbands along with disseminated magnetite crystals. The chert was actually made of tightly compacted polyhedrons of several micrometers in size without admixtures of other minerals (Fig. 1b). The SE mode image of anhedral hematite reveals micrometer-sized depressions on the surface (Fig. 1c) made probably by the coexisting minerals of micrometer scales. The in situ observation of the hematite bands in BSE mode also shows the existence of embedded micrometer-size chert nodules (black dots, Fig. 1d). Under high resolution, some hematite particles are platy hexahedrons of a few micrometers in size with straight boundaries between particles (Fig. 1e). In the same sample, anhedral hematite also appears in eroded-landform feature (Fig. 1f). The high-resolution STEM observation shows single hematite crystals of around 3–5 nm (Fig. 2a) with a SAED determined rhombohedral hematite structure ($R\bar{3}C$) (Fig. 2b).

Remarkable features preserved in hematite of Dales Gorge BIF are quartz nanocrystals (QNC). QNCs are observed in two modes: (1) as single crystals occupying either very shallow pits (Figs. 3a and 3b) or more developed pits or impact-like depressions with grooves or scratches (Figs. 3c, 3d, and 3e); and (2) cavities with one or two QNCs inside (Figs. 3f and 3g–3l). Figure 3g shows dense QNCs and empty pits scattered on the surface of hematite. Figures 3h, 3i, and 3j show surfaces of hematite with cavities either containing QNCs or remaining empty; in particular, Figure 3k demonstrates episodic QNC deposition by having QNCs in the lower-left part but without QNC in its upper-right part. Occasionally, small flake-like inclusions of 120 nm can also be observed adjacent to QNCs (Fig. 3l). A statistical assessment of 70 QNC yields an average of 170–100 nm for the long axis of particles and an average of 200–100 nm for the long-axis of associated pits. EDS analysis of a hematite breccia containing a QNC (Fig. 4a) shows only a weak peak of Si besides Fe and O peaks, implying a Si-O composition (Fig. 4b); similarly, the signal for Si cannot be detected on the surface of hematite breccia far from these quartz grains. The 120 nm flakes (Figs. 3k and 4c) are rare but represents the second mineral that can be found in hematite breccias. A weak Al shoulder peak (Fig. 4d) is shown without any other detectable metal as measured by EDS (detection limit is 0.1% atomic ratio). Because of the extremely low abundance of the flake-like mineral, its mineralogy cannot be determined by STEM. It may be the same Al-bearing phase previously suggested by Ahn and Buseck (1990) and Pecoits et al. (2009) to be Al on the structure of hematite. A STEM observed QNC grain of 250 nm from the residues of 6 M HCl treated hematite (Fig. 5a, bottom right) was further confirmed by SAED to be quartz in structure (Fig. 5b). The euhedral feature (Figs. 3b–3f) and the periodical structure (Fig. 5b) of these QNC particles distinguish their crystallographic habits from the abundant chert in BIFs. The chert from the residue of 6 M HCl treated hematite appear to be microcrystallites that show much smaller sizes than those of QNCs (Fig. 5c) with their average size of 32 ± 12 nm under STEM. These microcrystallites under high resolution STEM can only show diffuse circles by SAED (Fig. 5d), indicating long-range disorder, which is quite different from QNCs.

QNCs were only observed in the 2.48 Ga Dales Gorge BIF. The hematite from randomly selected BIFs of 3.0 Ga from Zimbabwe (Fedo and Eriksson 1996), 3.0–3.3 Ga of Fig Tree Group, Barberton of South Africa (Eriksson 1983), 2.52 Ga from North China (Zhai and Windley 1990), 2.4 Ga from Brazil (Klein and Ladeira 2000), 1874 Ma from Michigan (Schneider et al. 2000), and 1.8 Ga from North China (Zhai and Windley 1990) all were devoid of QNC (Figs. 6a–6f).

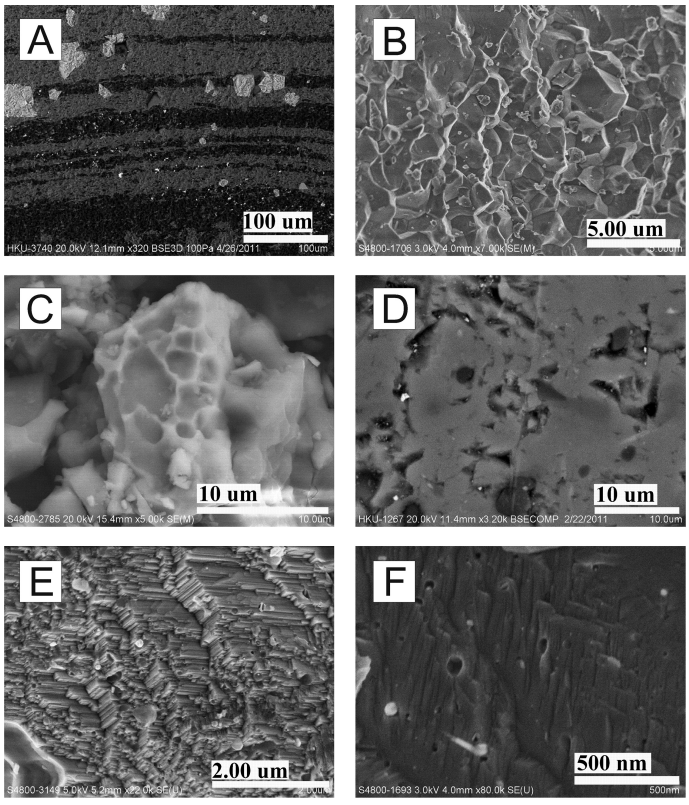

Figure 1. The chert (amorphous silica) and hematite bands in BIF. (**a**) The BSE mode image of chert (dark) and hematite (gray). The magnetite crystals (white) are disseminated in the matrix of chert and hematite; (**b**) feature of silica polyhedrons; (**c**) hematite surface with depressions of several micrometers in size; (**d**) the BSE image of anhedral hematite showing imbedded silica nodules and pits produced by magnetite crystals; (**e**) the aggregates of platy hematite; (**f**) the eroded landform-like surface of an anhedral hematite particle.

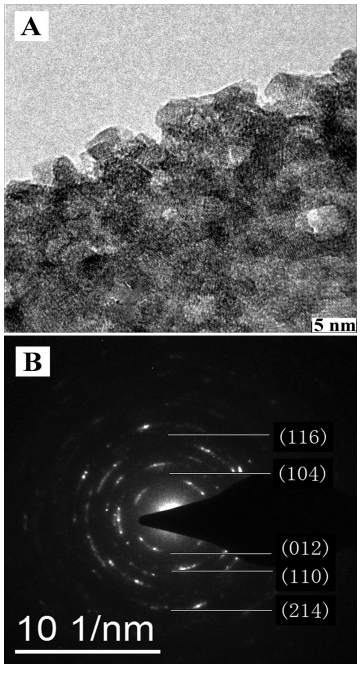

Figure 2. High-resolution TEM image of the ultrafine hematite crystals (**a**) and the SAED determined structure of hematite (**b**).

Discussion

In the entire BIF-assemblage, QNCs and (Si,Al)-containing flakes are the only minerals that can be found in hematite; all the other minerals, namely, magnetite, ferro-carbonate, minnesotaite, chert, and occasionally stilpnomelane are at least several micrometers in size and have sharp boundaries to hematite breccias. The ultrafine crystals of hematite (Fig. 2) and amorphous chert (Figs. 5c–5d) indicate the preservation of their early precipitating conditions (Ahn and Buseck 1990; Knauth 2005) and these observations also support that QNCs and (Si,Al)-containing flakes were originally deposited at the same time as the precursor of the nano-hematite. The fact that QNCs were only found in hematite breccias implies a hiatus between the deposition of hematite and those well crystallized BIF-minerals, which all contain Fe^{2+} in their structures. The hematite crystals occur only as 3–5 nm grains (Fig. 2a; Ahn and Buseck 1990) suggests that when these QNCs were deposited, the original oxyhydroxide, such as $Fe(OH)_3$ had transformed to hematite before consolidation (e.g., Krapež et al. 2003) because the transformation of mineral structures could alter or eliminate the observed "soft-sedimentary" fine structures.

Though hydrodynamically transported terrigenous sediments are rare in the BIFs (Ewers and Morris 1981; Trendall 2002), the occurrence of nano-quartz airborne "dusts" such as those from the distal subaerial volcanic eruptions might be explained

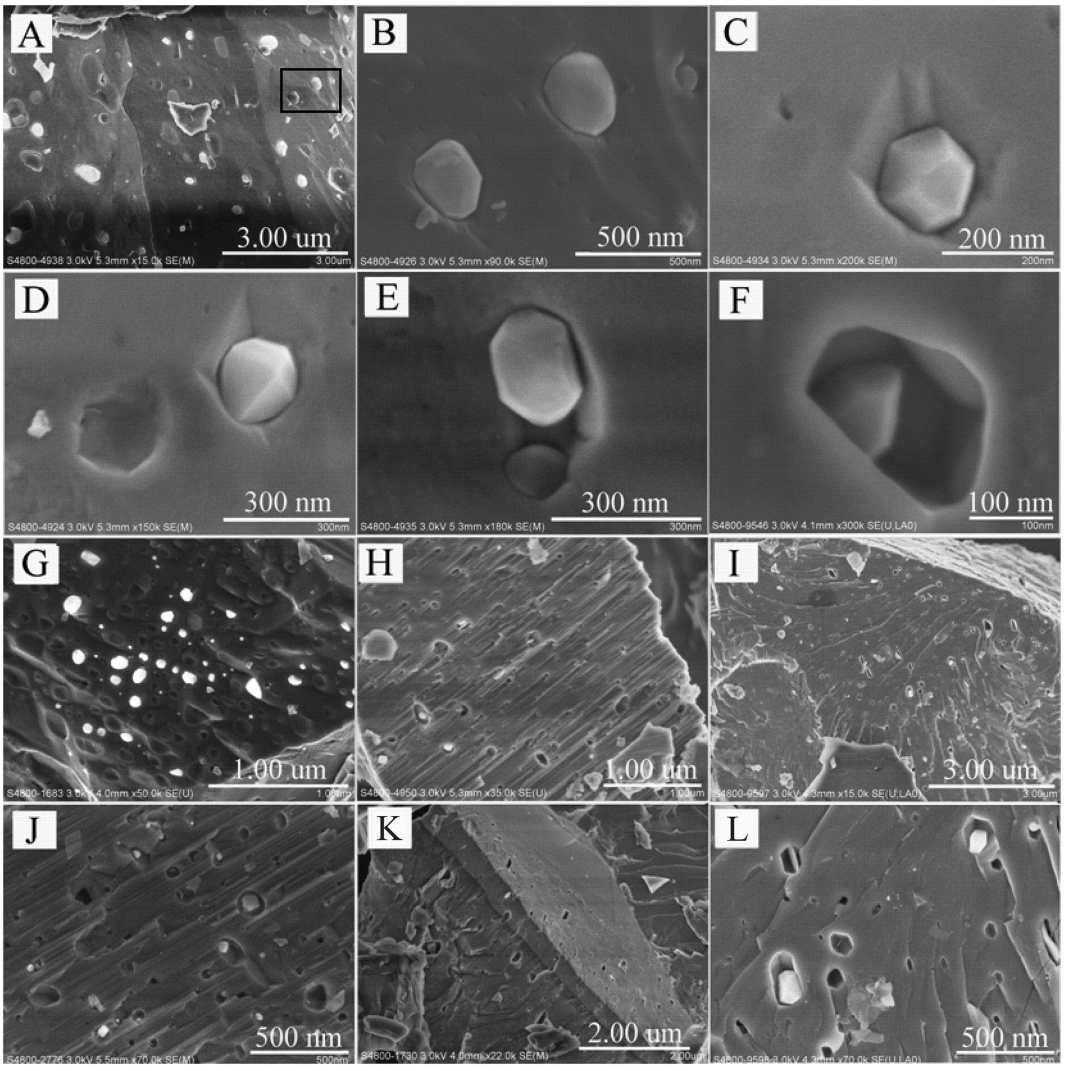

Figure 3. Euhedral QNCs and Al-containing flakes on the surface or in the hematite breccias. (**a**) A surface of hematite flake showing deposition of QNCs on the surface; (**b**) two QNCs amplified from the upper right of image **a**; (**c**) a QNC on the surface of hematite with falling scratches; (**d**) a QNC similar to c with a nearby empty pit; (**e**) a QNC amplified from the lower right part of image **a**; (**f**) a QNC in one deep pit; (**g**–**j**) various surfaces of hematite showed the existence of QNCs inside the hematite breccias; (**k**) a hematite breccia containing QNCs only in its lower-left part but no QNC in its upper-left part; (**l**) the surface of hematite showed the coexistences of QNC and flake-like crystals of similar size.

by the presence of QNCs in hematite of BIFs. Recent studies have inventoried the frequency of subaerial volcanic activities during the transition from the Archean to the Palaeoproterozoic that have been linked to the oxidation of the atmosphere (Kasting et al. 1993; Barley et al. 2005; Holland 2006; Kump and Barley 2007). Consistent with the subaerial volcanic eruption scenario, tuffaceous mudrocks rich in stilpnomelane volcanoclastics have been reported in the vicinity of Dales Gorge BIF in the Hamersley Basin (Pickard 2002; Trendall et al. 2004), indicating periods of episodic volcanism. The likelihood that (Si,Al)-containing flakes derived from the dissolution of the Al-containing stilpnomelane is not well founded because bundles of acicular stilpnomelane of ~20 μm in length were observed in some of the magnetite- and ankerite-rich thin mudrock layers in BIFs. The re-crystallization of amorphous silica to euhedral QNCs under diagenetic or metamorphic conditions does not seem plausible because no re-crystallization can be found in adjacent micrometer bands of chert, neither in macrobands of chert. The much smaller crystal sizes of these QNCs and their unique morphology also makes them different from the authigenic euhedral quartz (a few micrometers) that can crystallize at ambient temperature (e.g., MacKenzie and Gees 1971; Herdianita et al. 2000). For example, through interaction with an external thermal fluid, amorphous silica (and hematite) could recrystallize to much larger grains (>1 μm) under metamorphic conditions (<300 °C, Hippertt et al. 2001). On the contrary, the deposition of submicrometer airborne dusts, such as the volcanic nano-particles from the atmosphere diffused from a distance could be a reasonable source of the pyroclastic-derived QNC materials. The riverine transport of terrestrial material is unlikely because there is no

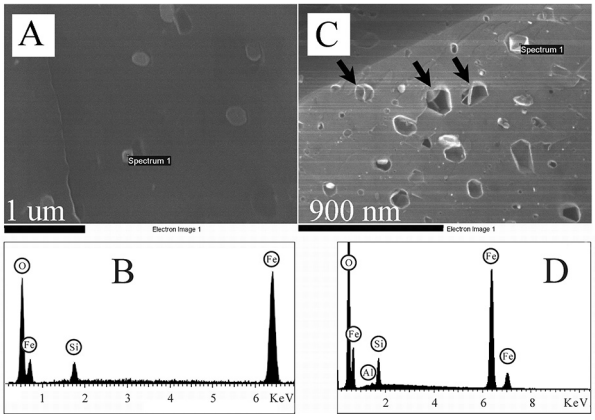

Figure 4. The chemical compositions of QNC and (Si,Al)-containing nanocrystals. (**a**) The surface of hematite containing QNCs for EDS analysis; (**b**) the EDS analysis showed a small Si peak beside Fe and O peaks; (**c**) the thin flakes in cavities (arrowed); (**d**) the EDS analysis of arrowed spots in image **c** showed Si and Al peaks beside Fe and O peaks.

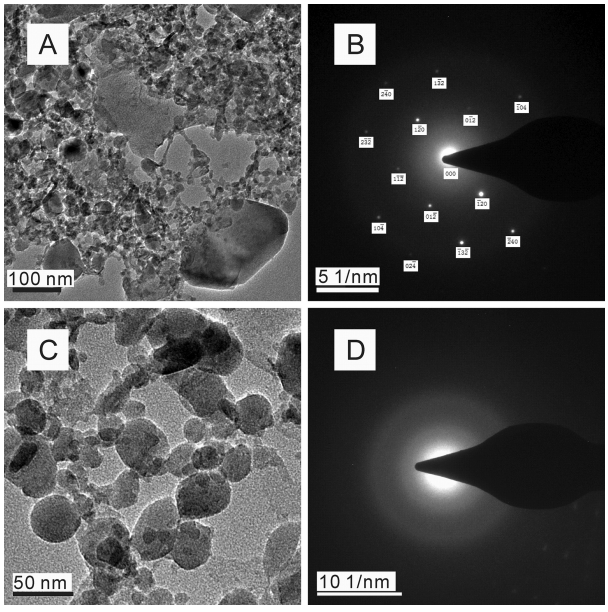

Figure 5. STEM determination of the structure of QNC. (**a**) QNC (bottom right) in the residue of the 6 M HCl treated hematite; (**b**) the SAED of QNC in **a** observed from zone axis of [421] indicated the structure of well-crystallized quartz; (**c**) chert microcrystallites under STEM; (**d**) the SAED pattern of chert in image **c** revealed their amorphous nature.

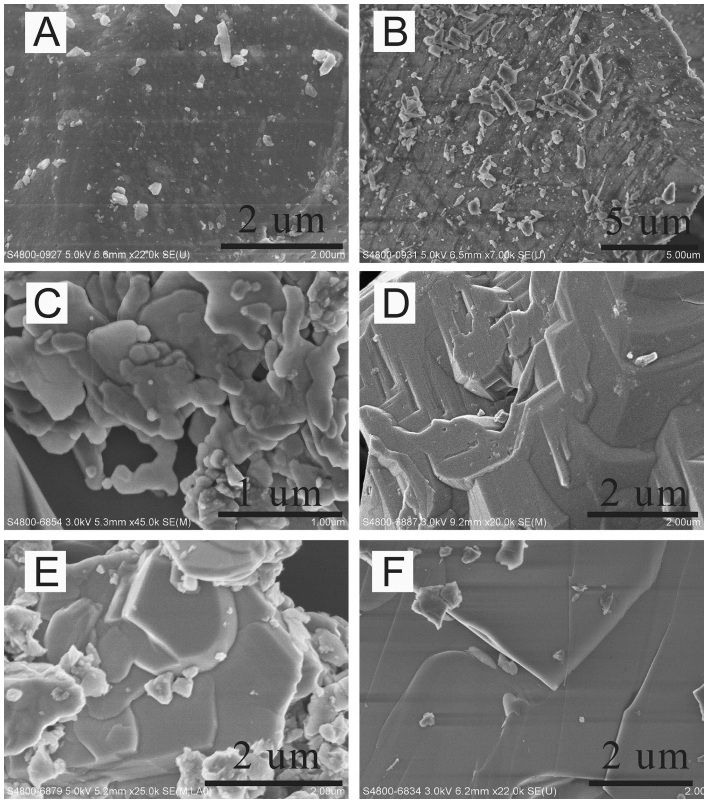

Figure 6. Selected hematite from BIF of different ages showing no QNC during their formations. (**a**) 1.8 Ga BIF from North China (Zhai and Windley 1990); (**b**) Michigan, 1874 Ma (Schneider et al. 2000); (**c**) Brazil, 2.4 Ga (Klein and Ladeira 2000); (**d**) 2.52 Ga BIF from North China (Zhai and Windley 1990); (**e**) South Africa, 3.0–3.3 Ga, (Eriksson 1983); (**f**) BIF from Zimbabwe, 3.0 Ga (Fedo and Eriksson 1996).

petrological evidence of the existence of weathered materials, nor any hydrodynamic features in the BIF (this study; Morris 1993; Trendall 2002).

The absence of QNC in other layers of Dales Gorge BIF suggests either a cessation of volcanism and/or widespread dispersion and dilution by deep water. However, we still cannot exclude the precipitation of QNCs in some other BIFs, or even the other parts of the examined samples because the deposition of QNCs is a highly momentary event when compared to the long depositional history of BIFs. According to Trendall et al. (2004), the integrated depositional rate of Dales Gorge BIF was about 5 m per million years, which means the transition from the QNC-containing hematite to hematite without QNCs shown in Figure 3k was only a matter of one year or so. Nevertheless, the presence of QNCs implies a hiatus between the precipitation of hematite and the formation of the other minerals in the BIF assemblage. In other words, the QNC became incorporated into the sediment during the earliest stages of diagenesis, and prior to the formation of later stage diagenetic or metamorphic minerals (e.g., magnetite and ferro-silicates). The Dales Gorge BIF, or more accurately, the hematite in it acted as a "repository" of QNCs derived from an airborne source, such as the eruption of local subaerial volcanoes (Pickard et al. 2004), because the transportation of authigenic quartz with weathered terrestrial source materials would preserve particles with varied size, possibly a somewhat rounded habit and complex mineralogy—features that are not observed in the studied BIF samples. This finding supports the contention that the Archean-Paleoproterozoic transition was a time when subaerial volcanism existed (Barley et al. 2005), and in this regard, we provide physical evidence in support of models that propose a link between changing tectonics, volcanism, and the redox composition of gases emitted into the atmosphere (Barley et al. 1997, 2005; Kump et al. 2001; Kump and Barley 2007).

Acknowledgments

Y.L.L. was supported by General Research Fund (HKU 703911) Research Grants Council of Hong Kong. K.K. acknowledges support from the Natural Sciences and Engineering Research Council of Canada. D.R.C. was supported by funds from the A.P. Sloan Foundation-sponsored Deep Carbon Observatory. We thank M. Darby Dyar for her great patience in editing and anonymous reviewers for their constructive reviews of our manuscript.

References cited

Ahn, J.H. and Buseck, P.R. (1990) Hematite nanospheres of possible colloidal origin from a Precambrian banded iron formation. Science, 250, 111–113.

Barley, M.E., Pickard, A.L., and Sylvester, P.J. (1997) Emplacement of a large igneous province as a possible course of banded iron formation 2.45 billion years ago. Nature, 385, 55–58.

Barley, M.E., Bekker, A., and Krapez, B. (2005) Late Archean to Early Paleoproterozoic global tectonics, environmental change and the rise of atmospheric oxygen. Earth and Planetary Science Letters, 238, 156–171.

Bau, M. and Dulski, P. (1996) Distribution of yttrium and rare-earth elements in the Penge and Kuruman Iron-Formations, Transvaal Supergroup, South Africa. Precambrian Research, 79, 37–55.

Campbell, I.H. and Allen, C.M. (2008) Formation of supercontinents linked to increases in atmospheric oxygen. Nature Geoscience, 1, 554–558.

Eriksson, K.A. (1983) Siliciclastic-hosted iron-formations in the early Archaean Barberton and Pilbara sequences. Journal of the Geological Society of Australia, 30, 473–482.

Ewers, W.E. and Morris, R.C. (1981) Studies of the Dales Gorge Member of the Brockman iron formation, Western Australia. Economic Geology, 76, 1929–1953.

Fedo, C.M. and Eriksson, K.A. (1996) Stratigraphic framework of the 3.0 Ga Buhwa greenstone belt: a unique stable-shelf succession in the Zimbabwe Archean craton. Precambrian Research, 77, 161–178.

Herdianita, N.R., Browne, P.R.L., Rodgers, K.A., and Campbell, K.A. (2000) Mineralogical and textural changes accompanying ageing of silica sinter. Mineral Deposita, 35, 48–62.

Hippertt, J., Lana, C., and Takeshita, T. (2001) Deformation partitioning during folding of banded iron formation. Journal of Structural Geology, 23, 819–834.

Holland, H.D. (2006) The oxygenation of the atmosphere and oceans. Philosophical Transactions of the Royal Society, B, 361, 903–916.

Kasting, J.F., Eggler, D.H., and Raeburn, S.P. (1993) Mantle redox evolution and the oxidation state of the atmosphere. Journal of Geology, 101, 245–257.

Klein, C. (2005) Some Precambrian banded iron-formations (BIFs) from around the world: their age, geological setting, mineralogy, metamorphism, geochemistry, and origin. American Mineralogist, 90, 1473–1499.

Klein, C. and Ladeira, E.A. (2000) Geochemistry and petrology of some Proterozoic banded iron-formations of the Quadrilatero Ferrifero, Minas Gerais, Brazil. Economic Geology, 95, 405–428.

Knauth, L.P. (2005) Temperature and salinity history of the Precambrian ocean: implications for the course of microbial evolution. Palaeogeography, Palaeoclimatology, Palaeoecology, 219, 53–69.

Krapež, B., Barley, M.E., and Kickard, A.L. (2003) Hydrothermal and resedimented origins of the precursor sediments to banded iron formation: sedimentological evidence from the Early Palaeoproterozoic Brockman Supersequence of Western Australia. Sedimentology, 50, 979–1011.

Kump, L.R. and Barley, M.E. (2007) Increased subaerial volcanism and the rise of atmospheric oxygen 2.5 billion years ago. Nature, 448, 1033–1036.

Kump, L.R., Kasting, J.F., and Barley, M.E. (2001) Rise of atmospheric oxygen and the "upside-down" Archean Mantle. Geochemistry Geophysics Geosystems, 2, DOI: 10.1029/2000GC000114.

La Berge, G.L. (1966) Altered pyroclastic rocks in iron-formation in the Hamersley Range, Western Australia. Economic Geology, 61, 147–161.

Li, Y.L., Konhuaser, K.O., Cole, D.R., and Phelps, T.J. (2011) Mineral ecophysiological evidence for biogeochemical cycles in an early Paleoproterozoic banded iron formation. Geology, 39, 707–710.

MacKenzie, F.T. and Gees, R. (1971) Quartz: synthesis at Earth-surface conditions. Nature, 173, 533–535.

Morris, R.C. (1993) Genetic modeling for banded iron-formation of the Hamersley Group, Pilbara Craton, Western Australia. Precambrian Research, 60, 243–286.

Pecoits, E., Gingras, M.K., Barley, M.E., Kappler, A., Posth, N.R., and Konhauser, K.O. (2009) Petrography and geochemistry of the Dales Gorge banded iron formation: paragenetic sequence, source and implications for palaeo-ocean chemistry. Precambrian Research, 172, 163–187.

Pickard, A.L. (2002) SHRIMP U-Pb zircon ages of tuffaceous mudrocks in the Brockman iron formation of the Hamersley Range, Western Australia. Australian Journal of Earth Sciences, 49, 491–507.

Pickard, A.L., Barley, M.E., and Krapez, B. (2004) Deep-marine depositon setting of banded iron formation: sedimentological evidence from interbedded clastic sedimentary rocks in the early Palaeoproteroaoic Dales Gorge Member of Western Australia. Sedimentary Geology, 170, 37–62.

Schneider, D.A., Bickford, M.E., Cannon, W.F., Schulz, K.J., and Hamilton, M.A. (2000) Age of volcanic rocks and syndepositional iron formations, Marquette Range Supergroup: implications for the tectonic setting of Paleoproterozoic iron formations of the Lake Superior region. Canadian Journal of Earth Sciences, 39, 999–1012.

Trendall, A.F. (2002) The significance of iron-formation in the Precambrian stratigraphic record. In W. Altermann, and P.L. Corcorane, Eds., Precambrian Sedimentary Environments: a Modern Approach to Depositional System, p. 33–66. Blackwell Publishing, Oxford.

Trendall, A.F. and Blockley J.G. (1970) The iron formation of the Precambrian Hamersley Group, Western Australia. Geological Survey of Western Australia Bulletin, 119, p. 365.

Trendall, A.F., Compston, W., Nelson, D.R., De Laeter, J.R., and Bennett, V.C. (2004) SHRIMP zircon ages constraining the depositional chronology of the Hamersley Group, Western Australia. Australian Journal of Earth Sciences, 51, 621–644.

Zhai, M. and Windley, B.F. (1990) The Archaean and early proterozoic banded iron formations of North China: their characteristics, geotectonic relations, chemistry and implications for crust growth. Precambrian Research, 48, 267–286.

Manuscript received April 23, 2012
Manuscript accepted December 18, 2012
Manuscript handled by M. Darby Dyar